

1 **The effect of erythrosine-B on the structuration of poloxamer 407 and cellulose**  
2 **derivative blends: *in silico* modelling supporting experimental studies**

3

4 Jéssica Bassi da Silva<sup>a</sup>, Katieli da Silva Souza Campanholi<sup>b</sup>, Gustavo Braga<sup>b</sup>, Paulo Ricardo  
5 de Souza<sup>b</sup>, Wilker Caetano<sup>b</sup>, Michael Thomas Cook<sup>c</sup>, Marcos Luciano Bruschi<sup>a,\*</sup>

6

7 <sup>a</sup>Postgraduate Program in Pharmaceutical Sciences, Laboratory of Research and Development  
8 of Drug Delivery Systems, Department of Pharmacy, State University of Maringa, Maringa,  
9 PR, Brazil.

10 <sup>b</sup>Department of Chemistry, State University of Maringa, Maringa, PR, Brazil.

11 <sup>c</sup>Research Centre in Topical Drug Delivery and Toxicology, Department of Pharmacy,  
12 Pharmacology, and Postgraduate Medicine, University of Hertfordshire, Hatfield, AL10 9AB,  
13 United Kingdom.

14

15

16

17

18

19

20

21

22 \*Corresponding author.

23 *E-mail address:* mlbruschi@uem.br (M.L. Bruschi).

24 **ABSTRACT**

25 Erythrosine is a dye approved for medical use that has shown promising photodynamic activity,  
26 allowing for the inactivation of microorganisms and activity against malignant cells. Despite  
27 the great photodynamic potential, erythrosine exhibits hydrophilicity, negatively impacting its  
28 action in biological membranes. Therefore, the incorporation of erythrosine in micellar  
29 polymeric systems, such as poloxamers, may overcome this limitation. Moreover, using  
30 bioadhesive and thermoresponsive polymers to combine *in situ* gelation and bioadhesion may  
31 enhance retention of this topically applied drug. In this work, mucoadhesive and  
32 thermoresponsive micellar systems were prepared containing erythrosine in two states: the  
33 native form (ERI) and the disodium salt (ERIs). The systems were evaluated based on the effect  
34 of ERI/ERIs on the micellar structure of the binary polymer mixtures. Optimised combinations  
35 of poloxamer 407 (polox407) and mucoadhesive sodium carboxymethylcellulose (NaCMC) or  
36 hydroxypropyl methylcellulose (HPMC) were used as micellar systems for ERI or ERIs  
37 delivery. The systems were studied with respect to theoretical interactions, qualitative  
38 composition, morphology, and micellar properties. *In silico* modelling indicated a higher  
39 interaction of the drug with poly(ethylene oxide) (PEO) than poly(propyleneoxide) (PPO)  
40 fragments of polox407. Systems containing NaCMC displayed a repulsive effect in the  
41 presence of erythrosine, due to the polymer's charge density. Both systems could convert the  
42 photosensitizer in its monomeric form, ensuring photodynamic activity. In these mixtures,  
43 crystallinity, critical micellar temperature and enthalpy of polox407 micellisation were  
44 reduced, and micellar size, evaluated by transmission electron microscopy (TEM), showed low  
45 impact of ERI/ERIs in HPMC preparations. Aiming toward photodynamic applications, the  
46 findings showed how ERI or ERIs can affect the micellar formation of gels composed of 17.5%  
47 (w/w) polox407 and 3% (w/w) HPMC or 1% (w/w) NaCMC, important for understating their  
48 behaviour and future utilisation as erythrosine delivery systems.

49 *Keywords:* gel, Pluronic F127, hydroxypropyl methylcellulose, sodium  
50 carboxymethylcellulose, erythrosine B, drug delivery.

51

## 52 **1. Introduction**

53 Erythrosine is a xanthene that has keen interest as a photosensitizer (PS) for  
54 photodynamic therapy (PDT). Its low toxicity combined with its history of use in dentistry and  
55 food products, makes the translation into the clinic easier than many other PS substances [1,2].  
56 In PDT, a luminous energy is absorbed by a PS and transferred to oxygen molecules, producing  
57 highly reactive cytotoxic species (particularly singlet oxygen  $^1\text{O}_2$ ) [3]. Erythrosine has been  
58 reported as dye to detect dental biofilms and has presented promising pharmacological activity  
59 in photodynamic inactivation of microorganisms and malignant cells [1,2,4].

60 The successful photodynamic activity is often related to the ability of a PS to present high  
61 visible light absorption and high singlet oxygen quantum yield ( $\Phi_{\Delta}^1\text{O}_2$ ), and erythrosine  
62 achieves satisfactory values in water (ca 0.62) [3]. The interaction between PS and membrane  
63 can have important bearing with the photodynamic activity, since the biological membranes  
64 are involved with its mechanism of action [5]. The incorporation of erythrosine in a micellar  
65 polymeric system, such as poloxamer-based preparations, could improve the delivery of this  
66 drug (log P of ERIs = -0.05 [6] and ERI= 0.46 [7]) to the cells with low changes in  
67 pharmacological performance of the drug itself as the native structure is retained. Moreover, it  
68 could control the release and improve retention of PS at the desired site, even considering  
69 highly humid regions such as the ocular or oral mucosal [8].

70 Poloxamers are a class of ABA triblock copolymer with the structure poly(ethylene  
71 oxide)(PEO)-*b*-poly(propylene oxide)(PPO)-*b*-PEO. Poloxamer 407 (polox407) is the most  
72 widely used copolymer in the development of thermoresponsive drug delivery systems due to  
73 its high performance, safety profile, and low-cost [9]. Poloxamer solutions exhibit critical  
74 micellisation temperatures (CMT), heating above which typically results in the formation of a  
75 spherical micelle with a hydrophobic PPO core and an hydrophilic PEO shell [10]. In  
76 appropriate concentration (above ca 15 %, w/v) and temperature, polox407 exhibits a reversible

77 transition from low concentration liquid to a viscous gel mesophase, a result of the micelles  
78 packing into a cubic liquid crystalline structure [11]. This property enables a cool solution to  
79 flow and become viscous when in contact with the body temperature, which is an important  
80 characteristic for topical formulations [12,13]. Above its CMT, polox407 switches to a face  
81 centered cubic structure of spherical core-shell micelles, as determined by small-angle neutron  
82 scattering [11]. Such systems present several advantages, alongside *in situ* gelation triggered  
83 by the body's heat, the high degree of well-ordered water allows for a smooth texture and the  
84 presence of micelles enables the solubilisation of both hydrophobic and hydrophilic drugs [14].

85         The combination of this thermoresponsive polymer with biomacromolecules opens the  
86 possibility of combining this *in situ* gelation with other functionality to construct novel  
87 nanocarriers in drug delivery systems [15]. The addition of mucoadhesive polymers such as  
88 poly(acrylic acid) derivatives [16–20] or cellulose derivatives [21–24] to polox407 systems  
89 have been extensively studied. They are able to combine thermoresponsive gelation of  
90 polox407 with improved adhesiveness of the polymer additives, however complex non-linear  
91 relationships are present in these systems which require careful optimisation [23]. Systems  
92 containing polox407 and HPMC or sodium NaCMC as mucoadhesive agents are promising  
93 with respect to their rheological, mechanical, micellar, and adhesive characteristics,  
94 particularly for topical drug delivery [21–26]. Although the structure of xanthene dyes shows  
95 several acid-base groups and that they may present several tautomeric forms, because of its  
96 pKa (around 2.35 and 3.79 [27]), erythrosine, at pH 7.0, exists in a predominantly dianionic  
97 form. However, considering the differences in log P and solubility of the protonated form (ERI)  
98 and its disodium salt (ERIs), changes in physicochemical and photophysical properties are,  
99 consequently, expected [27]. This study aimed to evaluate the effect of erythrosine in two  
100 different aggregation states (low solubility - ERI and high solubility - ERIs) on the structuration  
101 of thermoresponsive micellar systems, composed of polox407 and HPMC or NaCMC for



121 Systems were prepared by dispersion of 3% (w/w) HPMC or 1% (w/w) NaCMC in  
122 purified water, with stirring at room temperature. After the cellulose derivative was completely  
123 dispersed, 17.5% (w/w) polox407 was added to the preparation, and the mixture was stored at  
124 5 °C, for 48 h, ensuring complete wetting of the poloxamer. The polymeric system was then  
125 stirred again to complete dissolution of the remaining polymers. ERI or ERIs were added to  
126 the formulation at a level of 1% (w/w), with mechanical stirring, prior to the addition of  
127 polymers [2]. Final formulations were kept at 5 °C for at least 24 h prior to further analysis  
128 [29–31].

129

### 130 *2.3. Interaction studies supported by theoretical modelling*

#### 131 *2.3.1. Obtaining the association isotherm*

132 The interaction capacity of ERIs with polox407, polox407/NaCMC and  
133 polox407/HPMC micelles were performed by titration of aliquots of a stock solution of each  
134 system. The concentration of the solutions into the cuvette ranged from 0 to 1.4 % w/v for  
135 polox407, and from 0 to 0.12 % w/v for NaCMC or HPMC (keeping NaCMC or  
136 HPMC/polox407 ratio fixed at 0.07 at each addition) in a  $5.0 \times 10^{-7}$  mol.L<sup>-1</sup> of ERIs. All  
137 solutions were prepared in McIlvaine buffer (0.10 mol.L<sup>-1</sup>; pH 7.4) [32,33]. The interaction  
138 was monitored, at 35 °C, by acquiring the fluorescence emission spectra after the addition of  
139 polox407 or copolymer blends. The excitation used was 500 nm, reading from 520 nm to 750  
140 nm. The absorbance at excitation wavelength was less than 0.05 to avoid internal filter errors.

141

#### 142 *2.3.2. In silico modelling*

143 Molecular modelling studies of ERIs, ERIs/NaCMC, ERIs/HPMC,  
144 ERIs/NaCMC/polox407 and ERIs/HPMC/polox407, ERIs/PEO and ERIs/PPO were

145 performed in Orca 4.0 program [34] optimised in vacuum, employing Hartree-Fock (HF)  
 146 method with implementations for long range interactions (HF-3c), methodology developed to  
 147 obtain the most stable geometric structure in macromolecular systems [35]. The advanced  
 148 molecular editor Avogadro program version 1.1.1 (University of Pittsburgh, Department of  
 149 Chemistry, Pittsburgh, PA, USA.) was applied for graphical visualisation of the structures [36].

150

### 151 *3.2.3. Determination of complexation energy between copolymers fragments and ERIs* 152 *tautomers*

153 For the determinations of the complexation energy ( $\Delta E_{Comp}$ ) formed between ERIs and  
 154 the polymers studied, NaCMC (-NaCMC<sub>2</sub>-), HPMC (-HPMC<sub>3</sub>-) and proportional copolymer  
 155 fragments of PEO (-PEO<sub>12</sub>-), PPO (-PPO<sub>12</sub>-) and polox407 (-(PEO)<sub>5</sub>-(PPO)<sub>3</sub>-(PEO)<sub>5</sub>-) are  
 156 described in Eq. 1 for interactions between two components and Eq. 2 considering three  
 157 elements interaction [37].

$$158 \Delta E_{Comp} = E_{ERIs+polox407/Polymers/PEO/PPO} - (E_{ERIs} + E_{polox407/Polymers/PEO/PPO}) \quad (1)$$

159

$$160 \Delta E_{Comp} = E_{ERIs+polox407+Polymers} - (E_{ERIs} + E_{Polymers} + E_{polox407/PEO/PPO}) \quad (2)$$

161

162 where,  $E_{ERIs/polox407/Polymers/PEO/PPO}$  are the total electronic energy for the optimised  
 163 structures, considering the complex formed between ERIs, NaCMC and HPMC polymers, as  
 164 well as, the copolymers fragments of PEO, PPO and polox407 respectively.  $E_{ERIs}$ ,  $E_{Polymers}$ ,  
 165 and  $E_{polox407/PEO/PPO}$  are the individual electronic energy of the polymers and copolymers  
 166 fragments respectively used in the complexation process.

167



168 *2.4. Attenuated total reflectance Fourier transform infrared spectroscopy (ATR-FTIR)*

169 The infrared spectra were obtained by means of an Attenuated Total Reflectance (ATR)  
170 technique using an ATR-FTIR Nicolet iZ10 instrument (Thermo Fisher Scientific, EUA). All  
171 measurements were taken at room temperature (25 °C) on the zinc selenide (ZnSe) ATR crystal.  
172 The spectra were recorded over the range 4000-600 cm<sup>-1</sup>, at 4 cm<sup>-1</sup> resolution and represented  
173 by an average of 64 scans. The spectrum of the clean and dry ZnSe ATR crystal in ambient  
174 atmosphere was used as background for infrared measurement [38].

175

176 *2.5. Differential scanning calorimetry (DSC)*

177 Ca 35 mg of each formulation was placed in aluminum pans and hermetically sealed.  
178 The DSC was performed in a DSC Q20 (TA Instruments®, Surrey, United Kingdom) at a  
179 heating rate of 5 °C.min<sup>-1</sup> between 5 and 40 °C, under a nitrogen atmosphere. The CMT was  
180 determined from the associated endothermic peak in the DSC thermograms of the formulations,  
181 which occurred between 10 and 20 °C [24]. At heating rate of 5 °C/min between 0 to 400 °C,  
182 the polox407 crystallinity was calculated using DSC thermograms as the ratio of the measured  
183 polymer crystallisation enthalpy to the product of the polymer weight fraction and the  
184 crystallisation enthalpy of completely crystallized polox407 [39].

185

186 *2.6. Scanning electron microscopy (SEM)*

187 Samples were subjected to instant freezing using liquid nitrogen at -80 °C for 20 min.  
188 Frozen samples were then lyophilized for 48 h. Segments of the dried samples were carefully  
189 deposited on stubs containing double-sided adhesive carbon tape. The samples were metallised  
190 by the deposition of a thin layer of gold and evaluated by a SS550 Superscan Scanning Electron  
191 Microscopy (Shimadzu, Tokyo, Japan).

192

## 193 2.7. *Transmission electron microscopy (TEM)*

194 The TEM analysis was performed using a JEM-1400 Transmission Electron  
195 Microscope (JEOL, Tokyo, Japan), with an accelerating voltage of 120 kV. Samples were  
196 diluted 50-fold, and then negatively stained with 2% (w/v) uranyl acetate solution for  
197 observation. Samples were prepared at 37 °C to study the micelle formation. The measurements  
198 of the micelles by TEM were expressed as arithmetic mean and standard deviation of 250  
199 micelles of each system.

200

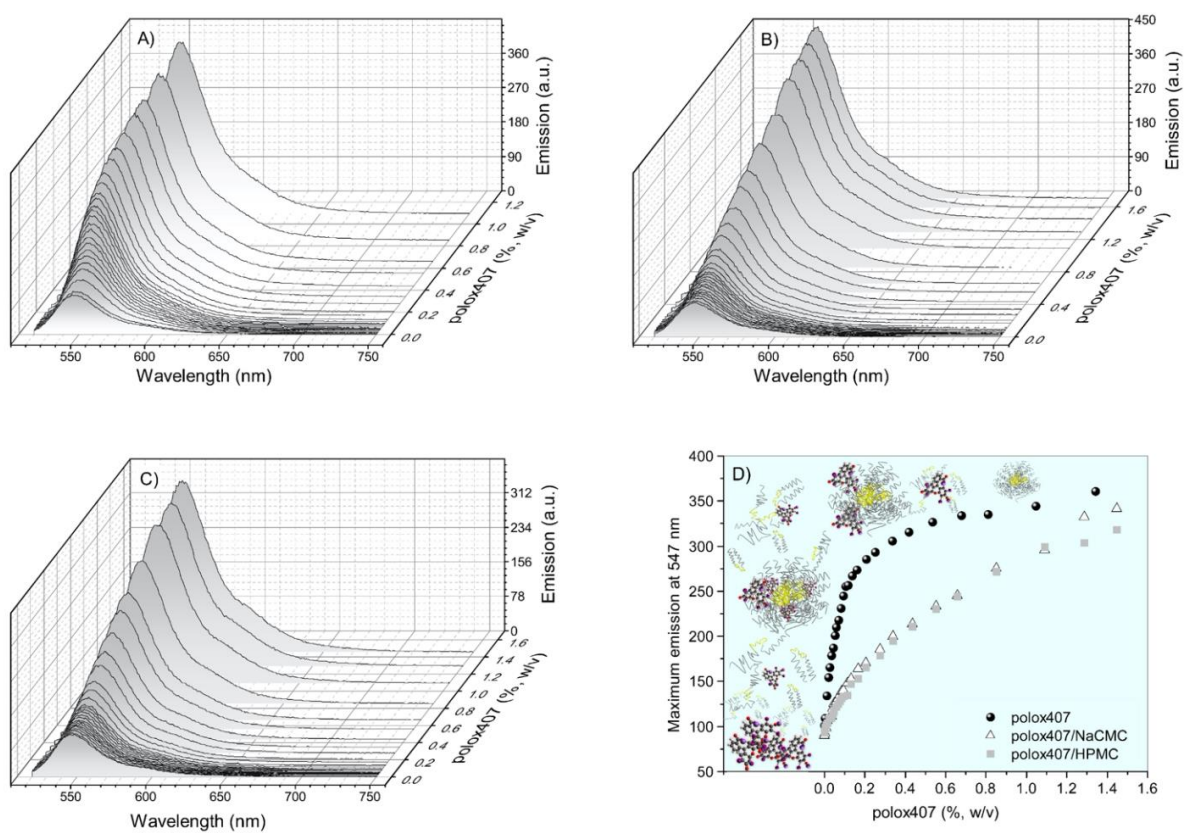
## 201 3. Results and discussion

### 202 3.1. *Interaction studies supported by theoretical modelling*

203 Xanthene photosensitizers, such as ERI/ERIs, show several acid-base groups. Thus, the  
204 pH of solution it is present in may determine physical-chemical properties [27]. The carboxylic  
205 group commonly shows higher acidity than the phenolic group; however, some inversion is  
206 expected depending on the structure of the studied compound. Although there are plenty of  
207 tautomeric structures for each proteolytic form, considering a pKa around 2.35 and 3.79  
208 described in the literature, both ERI and ERIs predominantly exist in their dianionic form at  
209 pH of 7.0 [27]. Considering the high solubility of ERIs in its complete dianionic state, this form  
210 was theoretically modelled with each polymer of the systems, improving the comprehension  
211 of the structure of the hydrogels.

212 The evaluation of the interaction and monomerisation of a PS compound in a micellar  
213 nanostructured system presents elevated relevance to predict formulation functionality in  
214 photodynamic therapy. The studies were carried out by obtaining the ERIs-micelle association  
215 isotherm (Fig. 2), achieved by monitoring the recovery of ERIs fluorescence by the effect of

216 gradual increase in polymer concentration. The high spectral overlap of monomers and small  
 217 aggregates formed makes electronic absorption studies unviable. Thus, the fluorescence  
 218 emission technique was selected due to its high sensitivity for detecting small aggregates,  
 219 similarly to the reported by Pellosi et al using the same PS [32,40]. The results were  
 220 complemented with molecular modelling, which provided important correlations when  
 221 employing the HF-3C method for structural optimisation.



222

223 **Fig. 2.** Interaction studies, at 35 °C, obtained by increasing the polymer (polox407, NaCMC  
 224 and HPMC) concentration on the ERIs in buffer solution (pH= 7.25): (A) polox407; (B)  
 225 polox407/NaCMC, (C) polox407/HPMC and (D) Isotherms of association. Graphs are  
 226 presented as ERIs emission vs. polox407 concentration. [NaCMC] = [HPMC] = 0 to 0.12 %  
 227 w/v; [ERI] =  $5.0 \times 10^{-7}$  mol.L<sup>-1</sup> ( $\lambda_{exc}$  = 500 nm, and monochromator slits excitation/emission  
 228 of 10/5, nm/nm).

229

230 Fig. 2A-C show low intensity of fluorescence emission of ERIs in an aqueous  
231 environment. This behaviour can be justified by the hydrophobic force of the carbon chain of  
232 PS, and its self-aggregated state (aggregates of small extension) in this solvent. It is known that  
233 self-aggregate are non-fluorescent species, and that collisions between PS and water molecules  
234 deactivate its excited state by non-radioactive processes (internal conversion) [41–43].  
235 However, as titration occurs, the polymer concentration increases and micelles of polox407 are  
236 formed after reaching the CMC for each system (values ranging from 0.0169 to 0.022 % w/v  
237 at 37 °C) [44]. When systems undergo micellisation, they are able to recover ERIs fluorescence  
238 intensity to a limit, where, theoretically, all drug molecules would be in their monomeric form  
239 (Fig. 2D). Moreover, as already described in the literature, alongside the increase of the  
240 fluorescence intensity, a bathochromic shift occurs (Fig. 2A-C). Thus, the peak of maximum  
241 emission changes from 547 nm to 556 nm, with measurements increasement of 9 nm in each  
242 case [45]. The spectral variations may suggest changes in the chemical environment, as ERIs  
243 partitions from water to the micellar microenvironment of reduced polarity [32]. The ERIs-  
244 water intermolecular interactions, that stabilize the PS fundamental state, are reduced with  
245 micellar incorporation. Thus, a reduction in the energy gap between fundamental and excited  
246 state produces the bathochromic shift observed [46].

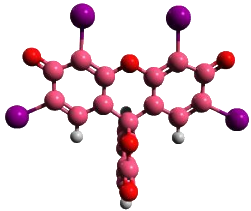
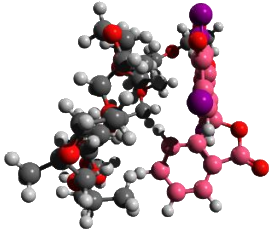
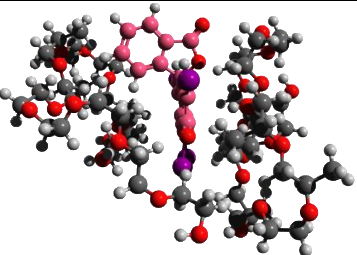
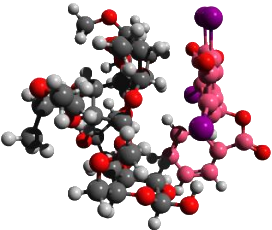
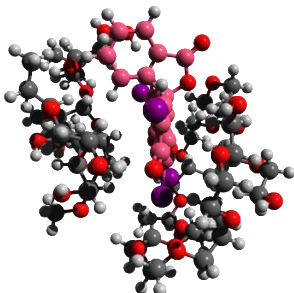
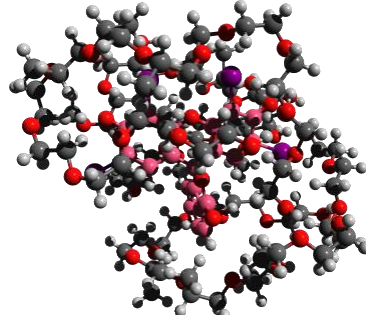
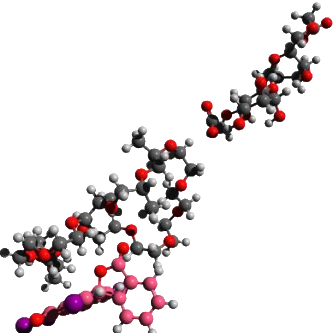
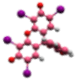
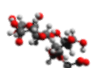
247 The results of computational modelling, displayed in Table 1, exhibit some tendency  
248 for ERIs partition into the polox407 micelles due to the favourable complexation energy  
249 ( $\Delta E_{Comp} = -44.47805379 \text{ kcal.mol}^{-1}$ ). The increase in the number of polox407 unimers makes  
250 the process even more favourable to ERIs incorporation ( $\Delta E_{Comp} = -70.29447533 \text{ kcal.mol}^{-1}$ ),  
251 reflecting the effect of the higher concentration of surfactant in this dynamic. Additionally,  
252 Table 2 demonstrates increased interaction of ERIs with PEO oligomers ( $\Delta E_{Comp} = -$   
253  $74.15897585 \text{ kcal.mol}^{-1}$ ) if compared to PPO ones ( $\Delta E_{Comp} = -15.2446224 \text{ kcal.mol}^{-1}$ ). The

254 results agree with the literature, which have shown the most efficient packing of this PS into  
255 the hydrated region of the micelle (PEO moieties). By Stern-Volmer constant it has been  
256 confirmed as well, with values of  $K_{sv} = 0.68 \text{ L.mol}^{-1}$  for ERIs [7]. Therefore, low values of this  
257 constant suggests ERIs is placed mainly in PEO region of the micelle [32].

258

259 **Table 1**

260 Total electronic energy for the optimised structures of erythrosine (ERIs) and polox407,  
261 NaCMC, HPMC or their mixture calculated at the HF-3c level of theory.

|                                                                                     |                                                                                                                                                                                  |
|-------------------------------------------------------------------------------------|----------------------------------------------------------------------------------------------------------------------------------------------------------------------------------|
| <b>ERIs</b>                                                                         | <b>ERIs/1polox407</b>                                                                                                                                                            |
| <i>HF-3c/hartrees</i> = -2314.46546376715                                           | <i>HF-3c/hartrees</i> = -4481.59083                                                                                                                                              |
| <sup>a</sup> $\Delta E_{\text{Comp}}/\text{kcal mol}^{-1}$ = -1452350.223           | <sup>a</sup> $\Delta E_{\text{Comp}}/\text{kcal mol}^{-1}$ = -44.47805379                                                                                                        |
|    |                                                                                                |
| <b>ERIs/2polox407</b>                                                               | <b>ERIs/1HPMC</b>                                                                                                                                                                |
| <i>HF-3c/hartrees</i> = -6648.720389                                                | <i>HF-3c/hartrees</i> = -4736.864382                                                                                                                                             |
| <sup>a</sup> $\Delta E_{\text{Comp}}/\text{kcal mol}^{-1}$ = -70.29447533           | <sup>a</sup> $\Delta E_{\text{Comp}}/\text{kcal mol}^{-1}$ = -44.83596244                                                                                                        |
|    |                                                                                                |
| <b>ERIs/1HPMC/1polox407</b>                                                         | <b>ERIs/1HPMC/2polox407</b>                                                                                                                                                      |
| <i>HF-3c/hartrees</i> = -6903.987973                                                | <i>HF-3c/hartrees</i> = -7928.622291                                                                                                                                             |
| <sup>a</sup> $\Delta E_{\text{Comp}}/\text{kcal mol}^{-1}$ = -88.20016883           | <sup>a</sup> $\Delta E_{\text{Comp}}/\text{kcal mol}^{-1}$ = -2002883.549                                                                                                        |
|  |                                                                                              |
| <b>ERIs/1NaCMC/1polox407</b>                                                        | <b>ERIs/1NaCMC</b>                                                                                                                                                               |
| <i>HF-3c/hartrees</i> = -5070.410046                                                | <i>HF-3c/hartrees</i> = -4045.82797                                                                                                                                              |
| <sup>a</sup> $\Delta E_{\text{Comp}}/\text{kcal mol}^{-1}$ = 716929.8552            | <sup>a</sup> $\Delta E_{\text{Comp}}/\text{kcal mol}^{-1}$ = 16.99276609                                                                                                         |
|  | <br><br> |

262

263 1 hartree = 627.5095 kcal.mol<sup>-1</sup>.

264 <sup>a</sup>For the calculations of  $\Delta E_{\text{Comp}}/\text{kcal mol}^{-1}$  were used the values from HF-3c/hartrees.

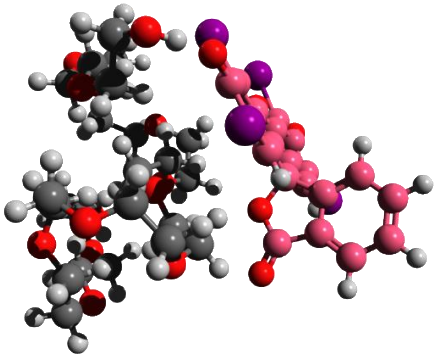
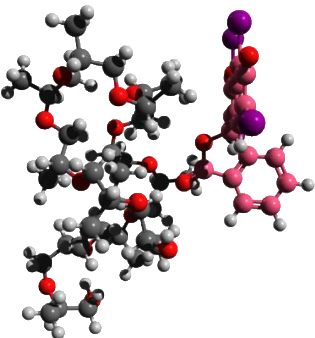
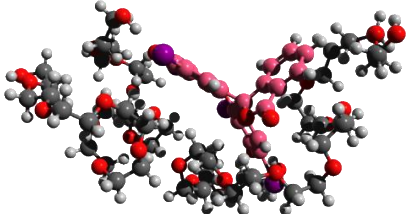
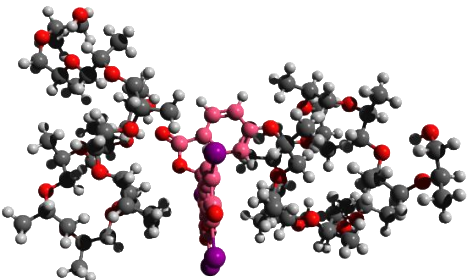
265

266 For the titration with polox407 solution (Fig. 2D), the saturation in fluorescence  
267 intensity was reached around 0.8 % (w/v). However, the ERIs binding isotherms presented  
268 reduced angles for the polox407/NaCMC and polox407/HPMC systems (Fig. 2D), without  
269 reaching complete saturation in the concentration range of surfactant evaluated. This behaviour  
270 can be justified by the higher hydration of the PEO segments when polox407 is mixed with  
271 cellulose derivative, in agreement with previously determined gelation [23] and CMT [24] for  
272 systems without drug. Thus, hydrated microenvironments may suppress the fluorescence of  
273 ERIs, besides changing its preferential microenvironment for accommodation. Evaluation  
274 involving titrations with NaCMC and HPMC, in the absence of polox407, were also performed.  
275 In these cases, a small interaction of ERIs with NaCMC polymeric systems was verified, with  
276 the slope of the association isotherm more inclined with HPMPC (Fig. S1). This effect is  
277 associated with NaCMC's negative charge in physiological pH, which repels the electronic  
278 density of the same nature for ERIs in this condition. Table 1 shows the preferable interaction  
279 of ERIs with HPMC ( $\Delta E_{Comp} = -44.83596244 \text{ kcal.mol}^{-1}$ ). As observed through the analysis,  
280 there is some separation degree between ERIs and NaCMC molecules ( $\Delta E_{Comp} =$   
281  $16.99276609/\text{kcal.mol}^{-1}$ ). The complexation energy of the systems containing  
282 ERIs/HPMC/polox407 presented negative energy ( $\Delta E_{Comp} = -88.20016883/\text{kcal.mol}^{-1}$ ), which  
283 highly decreases in the presence of two molecules of polox407 ( $\Delta E_{Comp} = -$   
284  $2002883.549/\text{kcal.mol}^{-1}$ ), indicating a minor impact of this mucoadhesive polymer on  
285 polox407 structuration in comparison to NaCMC, in presence of ERIs. On the other hand,  
286 systems composed of ERIs/NaCMC/polox407 may present higher solvation likely related to  
287 space promoted by the repulsion between charged species ( $\Delta E_{Comp} \text{ ERIs/NaCMC} > 0$ ). For  
288 instance, similar data have already been reported in the literature, ensuring low monomerisation  
289 capacity of ERIs in the presence of other anionic biomimetic systems, such as Sodium Dodecyl  
290 Sulphate (SDS) micelles [32].

291

292 **Table 2**

293 Total electronic energy for the optimised structures of erythrosine (ERIs) and fragments PEO  
 294 and PPO of polox407 calculated at the HF-3c level of theory.

| <b>ERIs/1PEO</b>                                                                    | <b>ERIs/1PPO</b>                                                                     |
|-------------------------------------------------------------------------------------|--------------------------------------------------------------------------------------|
| <i>HF-3c/hartrees</i> = -4213.291184                                                | <i>HF-3c/hartrees</i> = -4678.76299                                                  |
| <sup>a</sup> $\Delta E_{\text{Comp}}/\text{kcal mol}^{-1}$ = -53.86684692           | <sup>a</sup> $\Delta E_{\text{Comp}}/\text{kcal mol}^{-1}$ = -28.19099173            |
|   |   |
| <b>ERIs/2PEO</b>                                                                    | <b>ERIs/2PPO</b>                                                                     |
| <i>HF-3c/hartrees</i> = -6112.102021                                                | <i>HF-3c/hartrees</i> = -7043.062538                                                 |
| <sup>a</sup> $\Delta E_{\text{Comp}}/\text{kcal mol}^{-1}$ = -74.15897585           | <sup>a</sup> $\Delta E_{\text{Comp}}/\text{kcal mol}^{-1}$ = -15.2446224             |
|  |  |

295

296 1 hartree = 627.5095 kcal.mol<sup>-1</sup>297 <sup>a</sup>For the calculations of  $\Delta E_{\text{Comp}}/\text{kcal mol}^{-1}$  were used the values from HF-3c/hartrees.

298

299 Although some repulsion was found for NaCMC systems at molecular level, all the  
 300 binary systems showed satisfactory interaction, ensuring the monomerisation and  
 301 incorporation of ERIs in the micellar microenvironment. Studies at molecular level proved that  
 302 the platform combining polox407/NaCMC and polox407/HPMC presents sufficient  
 303 requirements to ensure adequate performance in PDT.



304

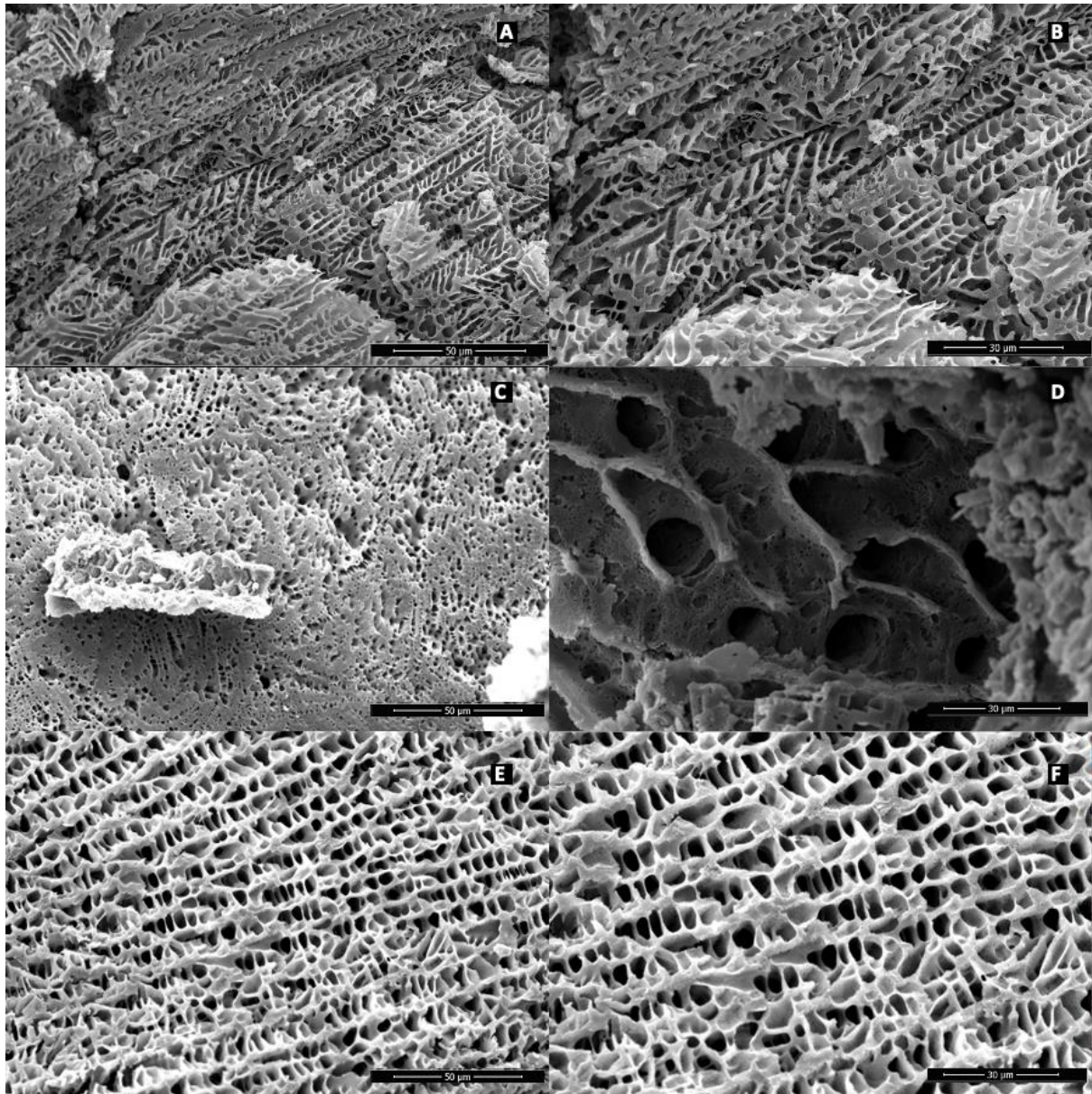
305 *3.2. Composition and morphological characterisation*

306 Polymeric systems' morphological analysis can provide a comprehension of their  
307 structure and organisation, aiding mechanistic understanding of the rheological  
308 characterisation [23]. Fig. 3 and 4 display SEM images of systems containing polox407 and  
309 HPMC or NaCMC in presence or absence of ERI or ERIs (at magnifications 2000 and 3000x).

310 In general, all formulations demonstrated clear network structure with differing pore  
311 size and quantity. Although heterogeneous, their morphology was well-defined, with  
312 conformation mainly attributed to the interactions between polar groups of micellar copolymer  
313 and cellulose derivatives [47]. Formulations containing polox407 and HPMC showed a  
314 lamellar layout in this dry state, which was retained into the presence of both ERI and ERIs  
315 (Fig. 3). ERI systems demonstrated amorphous morphology in comparison to ERIs, which may  
316 be given by its higher hydrophobicity, solubility balance, and self-aggregation ability [3],  
317 quoted by its amphiphilic log P 0.46 [7]. Among HPMC formulations, HPMC-ERIs was able  
318 to form numerous porous in comparison to the others. Since ERIs presents large solubility in  
319 water due to the predominance of the carboxylate form, it may establish strong ion-dipole  
320 interactions with water.

321

322



323

324 **Fig. 3.** Scanning electron microscopy (SEM) images of binary polymeric formulations  
 325 containing 17.5% (w/w) poloxamer 407 and 3% (w/w) hydroxypropyl methylcellulose, at  
 326 2000x magnitude (A) and 3000x magnitude (B), with 1% (w/w) erythrosine 95% purity (C and  
 327 D) or 1% (w/w) disodium salt erythrosine (E and F).

328

329 Formulations containing polox407 and NaCMC demonstrated a more porous  
 330 morphology. With a reduction of size accompanied by an increase in pore number, induced by  
 331 the addition of ERI or ERIs (Fig. 4). The addition of ERI or ERIs changed the organisation of

332 the system, which may be confirmed by computational modelling, where the complexation  
333 energy become extensively high ( $\Delta E_{\text{Comp}}/\text{kcal.mol}^{-1}$  of ERIs/NaCMC/1polox407 =  
334 716929.8552) when compared with the complexation energy of the same conditions of the  
335 system without ERI/ERIs ( $\Delta E_{\text{Comp}}/\text{kcal.mol}^{-1}$  of NaCMC/1polox407 = -32.71768652 [24]). The  
336 presence of drug may affect the micelle structure or the crystallisation of water during freezing.  
337 It may also induce the reduction of crystallinity of the polymers, providing morphological  
338 differences [13].

339 Dried formulations were also characterised by ATR-FTIR and DSC, as shown in Fig.  
340 5 and 6. The polox407 FTIR spectrum presented bands at 3420, 2870, and 1096  $\text{cm}^{-1}$  attributed  
341 to the  $-\text{OH}$  stretching, C–H aliphatic stretching, and C–O stretching [13,48], respectively. The  
342 band at 1645  $\text{cm}^{-1}$  is attributed to the  $-\text{OH}$  bending. NaCMC FTIR spectrum showed bands at  
343 1589 and 1414  $\text{cm}^{-1}$  attributed to  $-\text{COO}^-$  symmetric and asymmetric stretching, respectively  
344 [49]. Bands at 1322, 1103, and 1096  $\text{cm}^{-1}$  are ascribed to C–H stretching symmetric [50],  
345 primary, and secondary alcohols, respectively. In polox407/NaCMC FTIR spectrum (Fig. 5A),  
346 a band shifted at 1597  $\text{cm}^{-1}$  is observed in relation to that observed in the polox407 spectrum  
347 (1645  $\text{cm}^{-1}$ ), suggesting H–bonds between both polymers. Moreover, in the polox407/NaCMC  
348 FTIR spectrum, polox407 profile prevails due to the majority presence of this polymer into the  
349 system.

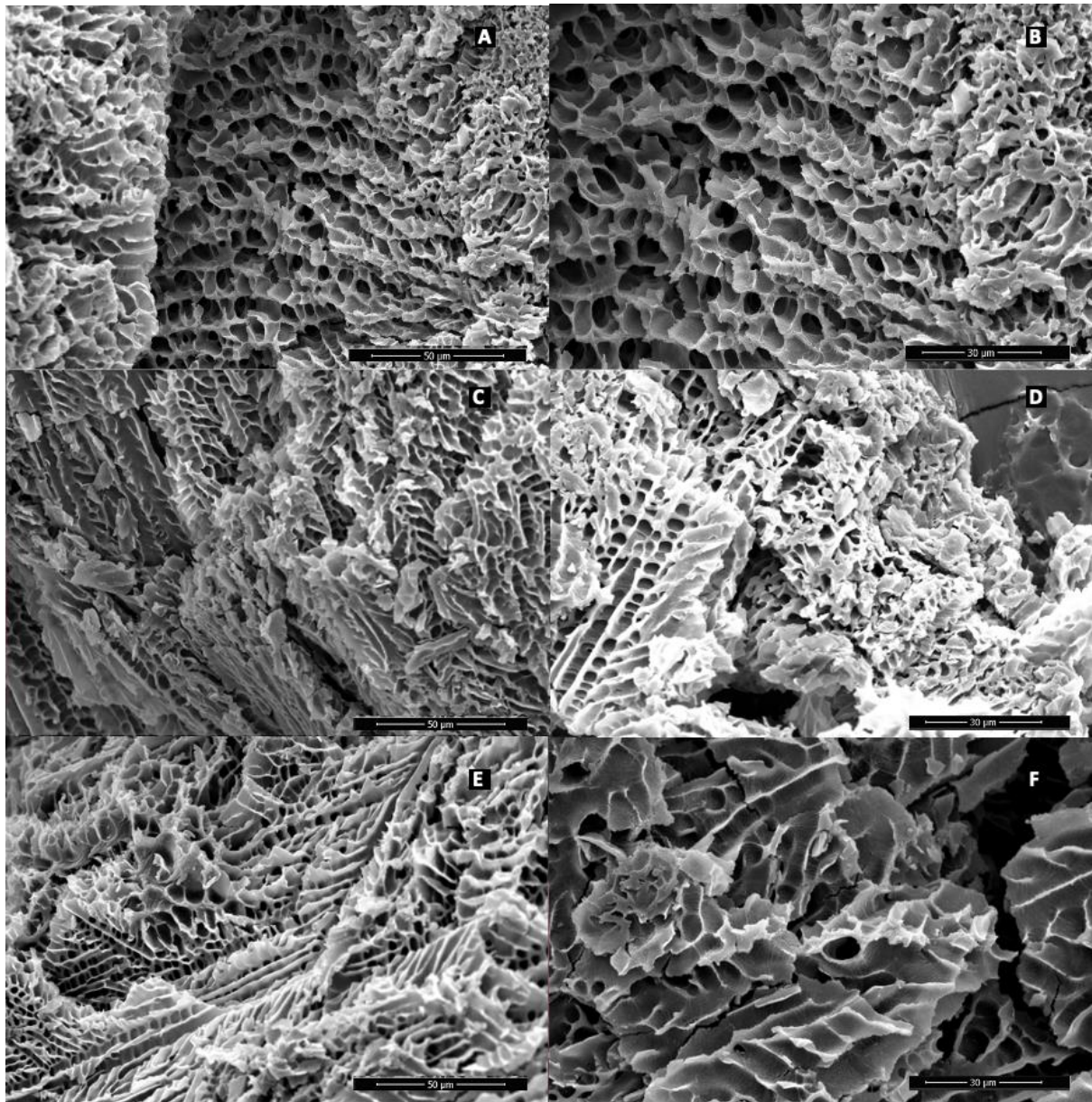
350 Fig. 5B displays HPMC FTIR spectrum, where bands around 2870  $\text{cm}^{-1}$  is linked to the  
351 C–H stretching vibration [48]. Bands at 1375, 1108, and 1043  $\text{cm}^{-1}$  are attributed to the C–H  
352 aliphatic stretching, primary and secondary alcohol, respectively. The slight broadening  
353 observed at 2870  $\text{cm}^{-1}$ , when polox407 is in presence of HPMC into polox407/HPMC gel may  
354 indicate C-H/C-H hydrophobic interactions between the polymeric chains. Furthermore, also

355 in polox407/HPMC spectrum, polox407 exhibited predominant bands due to its increased  
356 concentration into the preparation.

357 Fig. 5C-F presents the ERI and ERIs spectra and formulation containing both PS. The  
358 ERI FTIR spectrum present bands at 1600, 1543, and 1449  $\text{cm}^{-1}$  attributed to the benzene rings  
359 stretch [51]. Meanwhile, bands at 956 and 763  $\text{cm}^{-1}$ , were assigned to the C=C-H and aromatic  
360 ring's angular deformation, respectively. Bands at 1760, 1715, and 1405  $\text{cm}^{-1}$ , in ERI spectrum,  
361 were attributed to the carboxylic acid C=O stretching, C=O stretching of conjugate acid, and  
362 -OH bending of carboxylic acid, respectively. Although ERIs FTIR spectrum (Fig. 5C and D)  
363 exhibited similar bands to that observed in the ERI FTIR spectrum, ERIs did not display the  
364 bands at 1760, 1715, and 1405  $\text{cm}^{-1}$  due to the disodium salt form of this PS. Indeed, as  
365 observed in the FTIR spectra, ERI or ERIs were incorporated in the formulations.

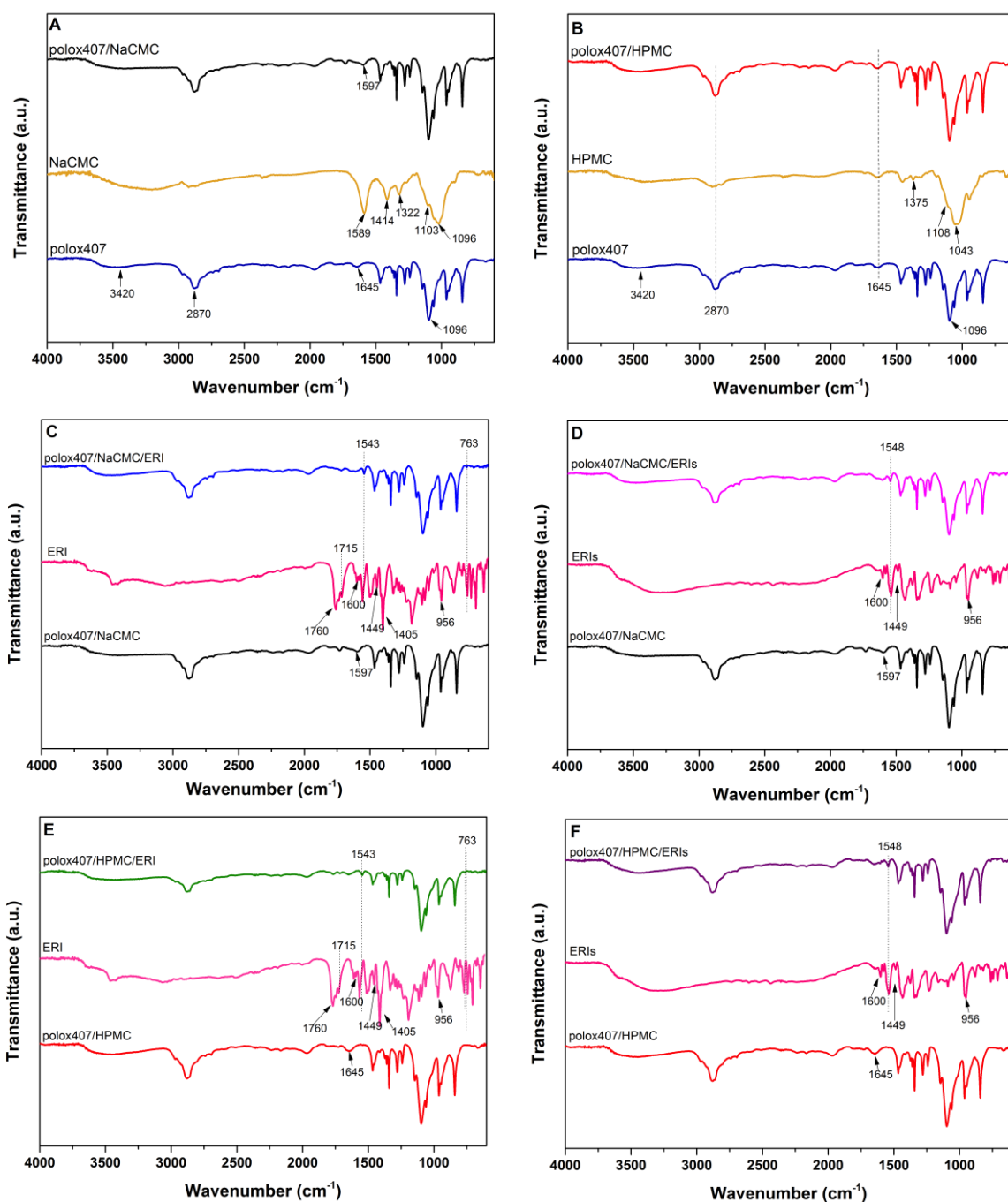
366 .





367

368 **Fig. 4.** Scanning electron microscopy (SEM) images of binary polymeric formulations  
369 containing 17.5% (w/w) poloxamer 407 and 1% (w/w) sodium carboxymethylcellulose at  
370 2000x magnitude (A) and 3000x magnitude (B), with 1% (w/w) erythrosine 95% purity (C and  
371 D) or 1% (w/w) disodium salt erythrosine (E and F).



372

373 **Fig. 5.** Attenuated total reflectance Fourier transform infrared spectroscopy (ATR-FTIR)  
 374 spectra of the binary polymeric formulations of 17.5% (w/w) poloxamer 407 (polox407) and  
 375 3% (w/w) hydroxypropyl methylcellulose (HPMC, B, E and F) or 1% (w/w) sodium  
 376 carboxymethylcellulose (NaCMC, A, C and D) without or with erythrosine 95% purity (ERI,  
 377 E and F) or disodium salt erythrosine (ERIs, C and D).

378 DSC thermograms of the dried formulations with or without drug are displayed in Fig.  
379 6. The formulations show an endothermic peak at 55.2 °C, which is associated with the  
380 polox407 copolymer melting point [24,52,53], revealing the presence of polox407 in its  
381 crystalline state when in the presence of both cellulose derivatives. The enthalpy associated  
382 with endotherm melting transition decreased in the presence of the drugs (Table 3), whereas  
383 the peak position remained approximately unaltered. The addition of cellulose derivatives  
384 plasticize polox407, since a decrease in its crystallinity occurs [24]. This could be related to  
385 interaction between both polymers [54], which was already detected by rheology [23].  
386 Comparing polox407 crystallinity into the mixture with and without drug (Table 3), there is a  
387 reduction of this property when ERIs is added on it, while ERI promoted an increase of it. The  
388 presence of ERIs seems to disturb the formation of the ordered crystalline structure of polox407  
389 chains in both systems. Meanwhile, ERI facilitated an ordered association of the copolymer  
390 molecules. Additionally, the exothermic peak observed near to 150 °C for the preparation  
391 without drug and containing ERIs, was not exhibited for samples with ERI, indicating the  
392 favourable organisation of polox407 crystallinity may result in a unique crystalline form.

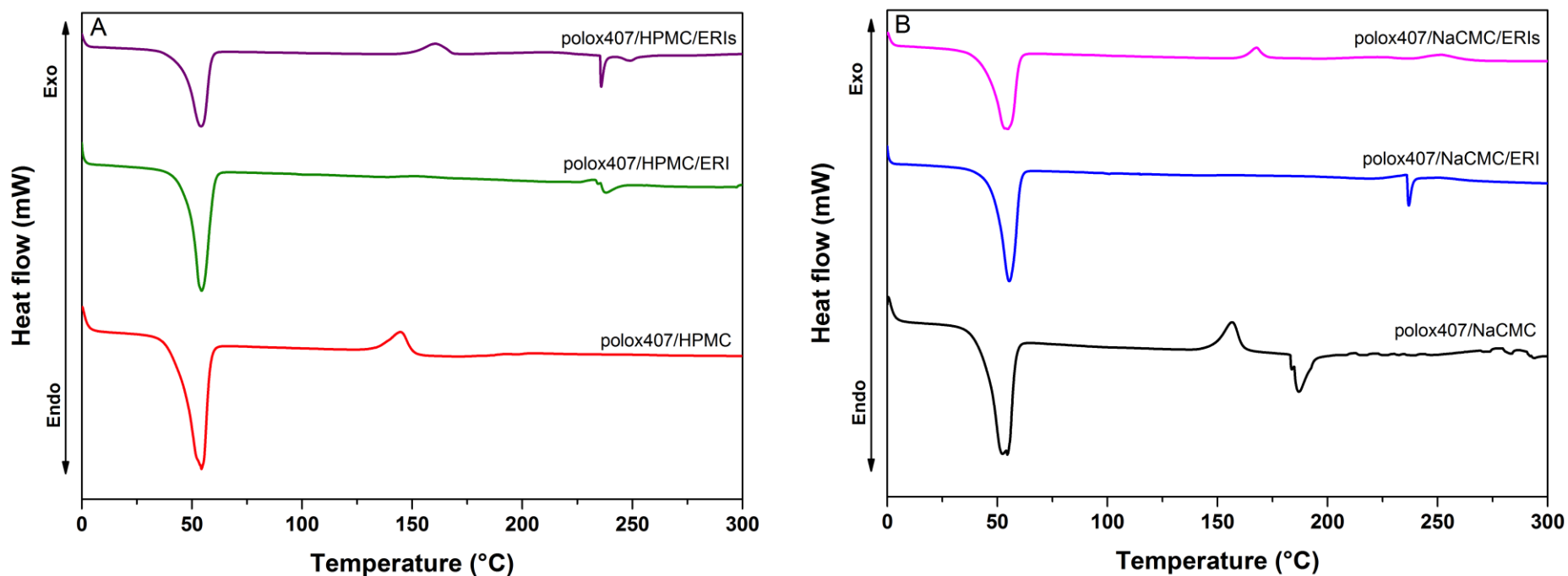
393 **Table 3**

394 Differential scanning calorimetry (DSC) crystallinity of pure poloxamer 407 (polox407) polymer and mixtures composed of 17.5% (w/w) polox407  
 395 and 1% (w/w) sodium carboxymethylcellulose (NaCMC) or 3% (w/w) hydroxypropyl methylcellulose (HPMC), without or with 1% (w/w) ERI  
 396 or ERIs.

| Formulation         | Cellulose derivative<br>fraction | Drug<br>fraction | polox407<br>weight fraction | Enthalpy<br>(J/g) | polox407 crystallinity<br>(%) | Crystallinity reduction<br>(%) |
|---------------------|----------------------------------|------------------|-----------------------------|-------------------|-------------------------------|--------------------------------|
| polox407            | 0.000                            | 0.000            | 1.000                       | 112.20            | 100.00                        | 0.00                           |
| polox407/HPMC       | 0.146                            | 0.000            | 0.854                       | 84.65             | 88.38                         | 11.62                          |
| polox407/HPMC/ERI   | 0.146                            | 0.010            | 0.814                       | 87.69             | 96.02                         | 3.98                           |
| polox407/HPMC/ERIs  | 0.146                            | 0.010            | 0.814                       | 82.06             | 89.85                         | 10.15                          |
| polox407/NaCMC      | 0.054                            | 0.000            | 0.946                       | 75.74             | 71.36                         | 28.64                          |
| polox407/NaCMC/ERI  | 0.054                            | 0.010            | 0.897                       | 88.73             | 88.12                         | 11.88                          |
| polox407/NaCMC/ERIs | 0.054                            | 0.010            | 0.897                       | 84.13             | 83.55                         | 16.44                          |

397





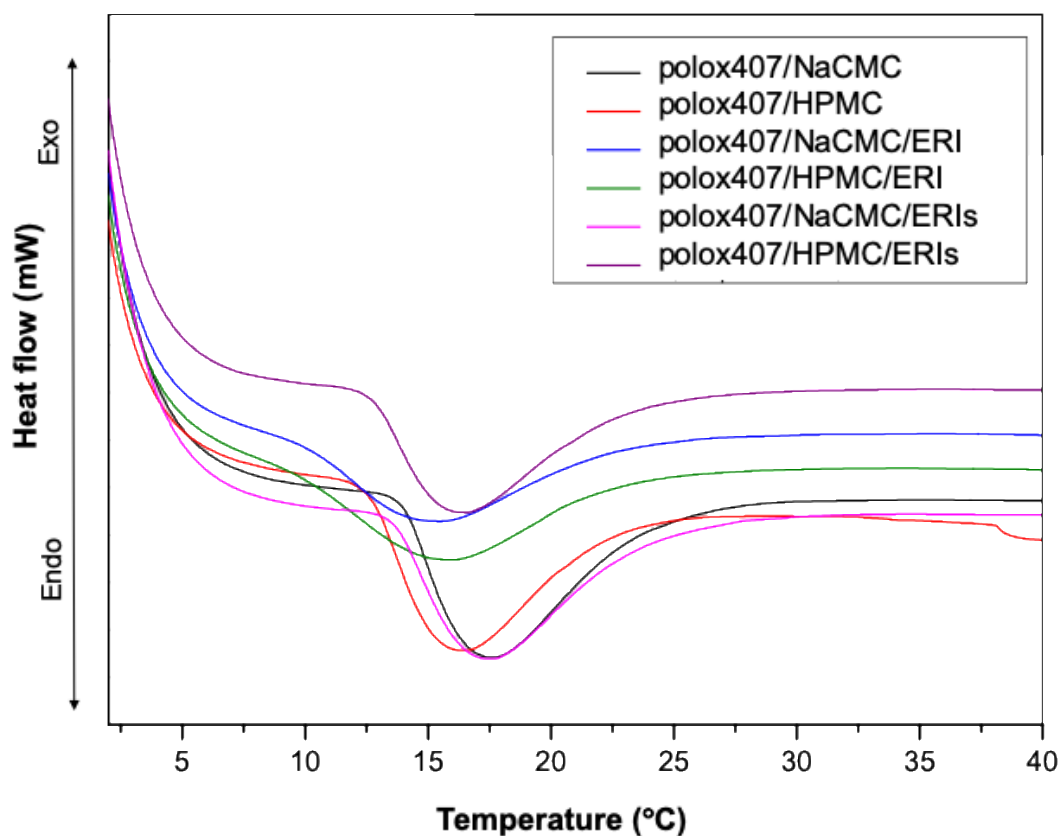
398

399 **Fig. 6.** Differential scanning calorimetry (DSC) thermograms of dried binary polymeric systems containing (A) poloxamer 407 (polox407) and  
 400 hydroxypropyl methylcellulose (HPMC) or (B) sodium carboxymethylcellulose (NaCMC) without or with erythrosine 95% purity (ERI) or  
 401 disodium salt erythrosine (ERIs).

402

### 403 3.3. *Micellar characterisation*

404 The DSC analysis of the gels allows for the characterisation of nanostructured systems,  
405 providing detailed information regarding enthalpy associated with thermally-induced events  
406 [55]. It may be used alongside the study of self-assembly behaviour of polox407, since micellar  
407 domain formation is a crucial step for gelation of systems containing this thermoresponsive  
408 polymer [56]. Therefore, the CMT of the systems with or without drug was determined by DSC  
409 (Fig. 7). The endothermic peaks demonstrate the desolvation of hydrophobic PPO block of  
410 polox407 with increasing temperature. As this phenomenon is responsible for micelle  
411 formation, the peak of this calorimetric event may be considered as the CMT of the  
412 preparations [57]. As reported in the literature, the CMT of HPMC/polox407 was found around  
413 16.7 °C, whilst NaCMC/polox407 preparations exhibited a CMT of 17.8 °C [24]. HPMC  
414 preparations with ERI presented a CMT of 16.0 °C, while ERIs preparations demonstrated  
415 CMT at 16.4 °C. NaCMC systems with ERI or ERIs demonstrated CMTs of 15.4 °C and 17.5  
416 °C, respectively.



417

418 **Fig. 7.** Differential scanning calorimetry (DSC) thermograms of binary polymeric hydrogels  
 419 composed of poloxamer 407 (polox407) and hydroxypropyl methylcellulose (HPMC) or  
 420 sodium carboxymethylcellulose (NaCMC) without or without of 1% (w/w) erythrosine 95%  
 421 purity (ERI) or 1% (w/w) disodium salt erythrosine (ERIs).

422

423 The addition of drug decreased the CMT of both polymeric systems, which can be  
 424 mechanistically interpreted through several viewpoints. In part, the presence of co-solute alters  
 425 the amount of water available to solvate polox407 chains. ERI reduced this temperature to a  
 426 greater extent than ERIs, with this effect more pronounced in NaCMC preparations. This  
 427 agrees with computational analysis, which found that the NaCMC/polox407 system containing  
 428 ERI has high solvation, since there is a large distance between the charged species ( $\Delta E_{\text{Comp}}$   
 429 ERI/NaCMC > 0). Whilst a negative entropy contribution is driving force for the micellisation

430 of polox407 block copolymer [58], direct interactions between cellulose derivatives and  
 431 copolymer may contribute with changes in either thermodynamic parameters, altering CMT  
 432 [24]. The literature reports a CMT for pure 20% (w/w) polox407 dispersions at about 12 °C  
 433 [56,59], and an enthalpy of micellisation of  $25.5 \pm 2$  J/g for polox407 [60,61]. Compared to a  
 434 polox407 solution, both cellulose derivatives reduced the CMT and enthalpy of micellisation  
 435 of polox407 (Table 4), reflecting a decline in the energy consumed for PPO dehydration [62].  
 436 Although mixtures between ERI and polox407 have been reported with relative low bonding  
 437 ability, with the dye being located in PEO region [3], the results suggest that hydrophobic  
 438 interactions between PPO blocks and aliphatic backbone of drug and cellulose derivatives may  
 439 promote PPO nanophase separation, requiring less energy for dehydration [62]. ERI  
 440 demonstrated significant reduction of enthalpy which is likely related to its relatively high  
 441 hydrophobicity and therefore reduced interaction with water or, perhaps, a tendency of  
 442 interaction with PPO, in comparison to ERIs [24,63,64]. For instance, the literature reports, by  
 443 differences between erythrosine pKa in water and in polox407 solution, that its carboxylic  
 444 group establishes interactions with PEO groups while phenyl ring is accommodated in PPO  
 445 inner region [65].

446

447 **Table 4**

448 Micellisation enthalpy of hydrogels containing 17.5% (w/w) polox407 and 1% (w/w) sodium  
 449 carboxymethylcellulose (NaCMC) or 3% (w/w) hydroxypropyl methylcellulose (HPMC),  
 450 without or with 1% (w/w) ERI or ERIs obtained by DSC.

| Formulations               | Concentration<br>(%, w/w) | T <sub>onset</sub><br>(°C) | T <sub>peak</sub><br>(°C) | Micellisation enthalpy<br>(J/g of polox407) |
|----------------------------|---------------------------|----------------------------|---------------------------|---------------------------------------------|
| polox407/HPMC <sup>a</sup> | 17.5/3                    | 12.5                       | 16.7                      | 17.91                                       |

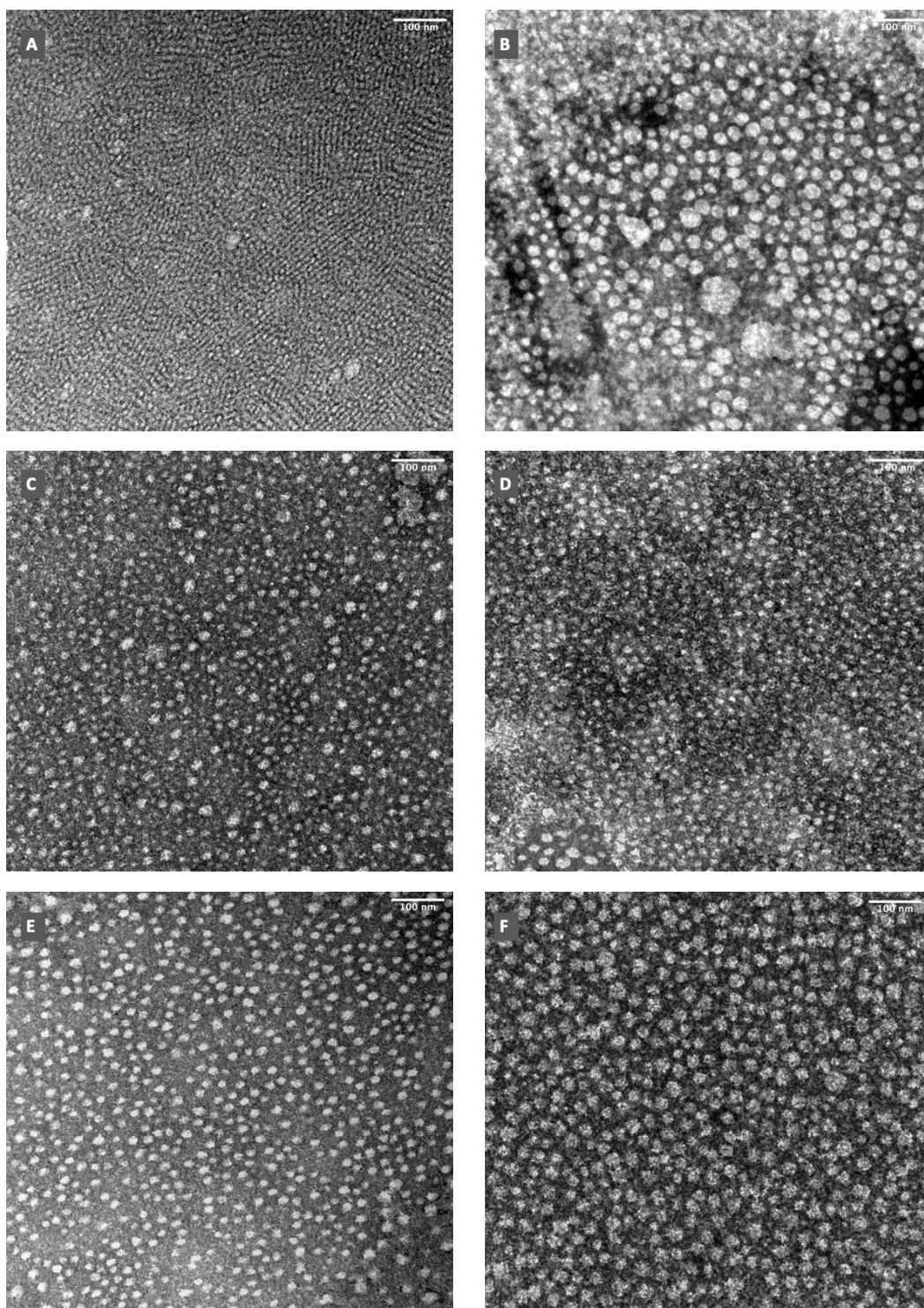
|                             |          |      |      |       |
|-----------------------------|----------|------|------|-------|
| polox407/HPMC/ERI           | 17.5/3/1 | 10.7 | 16.1 | 10.53 |
| polox407/HPMC/ERIs          | 17.5/3/1 | 12.8 | 16.2 | 13.65 |
| polox407/NaCMC <sup>a</sup> | 17.5/1   | 14.0 | 17.7 | 15.53 |
| polox407/NaCMC/ERI          | 17.5/1/1 | 10.8 | 15.6 | 10.29 |
| polox407/NaCMC/ERIs         | 17.5/1/1 | 13.7 | 17.5 | 17.69 |

---

451           <sup>a</sup>[24]

452

453



454

455 **Fig. 8.** Transmission electron microscopy (TEM) images of formulations comprising  
456 poloxamer 407 and hydroxypropyl methylcellulose (A) with erythrosine 95% purity (C) or  
457 disodium salt erythrosine (E) and poloxamer 407 and sodium carboxymethylcellulose (B) with  
458 erythrosine 95% purity (D) or disodium salt erythrosine (F) at 37 °C (A). Original  
459 magnification x100,000.

460 TEM micrographs allow for the determination of micelle size and shape by direct  
461 observation. Images of all six systems, dried at 37 °C, are displayed in Fig. 8. The individual  
462 organisation with spherical shape was observed, in line with the literature [24,66], reflecting  
463 the micellar organisation of polox407 and its triblock structure [66]. HPMC system without  
464 drug had a micelle diameter of  $13.4 \pm 2.3$  nm. The measurements show the absence of  
465 significant changes in the size among HPMC formulations, agreeing with theoretical  
466 modelling, which demonstrated a minor impact on polox407 structuration. Meanwhile,  
467 NaCMC system without drug had an average diameter of  $25.5 \pm 4.5$  nm. With ERIs, expressive  
468 changes was not observed, with average diameter of  $21.5 \pm 9.8$  nm. However, the ERI  
469 incorporation showed a trend to reduced values, with micelles diameter close to  $14.4 \pm 7.3$  nm.  
470 Overall, the images revealed a high heterogeneity of size in NaCMC preparations, which  
471 negatively impacts micellar packing, as observed by DSC and *in silico* modelling of the  
472 hydrogels [56].

473 The location of xanthene dyes by fluorescence quenching experiments have been  
474 reported with some preference of ERIs to be positioned in PEO segments of polox407, when  
475 in its raw dispersion [3], agreeing with the *in silico* model. This justifies the small contraction  
476 tendency observed for the ERIs system, since micellar clusters and heterogeneity of size are  
477 frequently linked to changes in the shell [56]. However, the trend to reduction exhibited for  
478 ERI in NaCMC preparations, may be indicative of stronger interaction with PPO fragment  
479 (drug molecules in the aggregate state due to the solubility equilibrium) driving collapse of  
480 the micelle core (in accordance with CMT measurements). Although ERI has a relatively  
481 amphiphilic profile ( $\log P$  0.46) [7], its backbone and self-aggregation in water [27] may favour  
482 its interaction with PPO core, reducing micelle size of NaCMC system in comparison to the  
483 raw blend. For instance, the literature reports the presence of hydrophobic drug molecules,



484 such as naproxen and indomethacin in polox407 solution decreases its micellar size and  
485 aggregation number [67,68].

486           Although most of literature report a pKa around 2.35 for the carboxylic group of ERI  
487 and 3.79 for the phenolic group, some authors have found different values [27]. Erythrosine  
488 pKa may change depending on the chemical environment the dye is placed. For instance,  
489 Freitas et al. demonstrated the pKa of erythrosine increases in polox407 solutions with pKa  
490 inversion observed ( $pK_{aOH} < pK_{aCOOH}$ ), giving values of 6.54 for the carboxylic group and  
491 2.17 for phenolic groups [65]. That is linked to the presence of oxyethylene groups in the  
492 external portion of the micelle, which are able to attract positive charges to its surface,  
493 increasing pKa values, since negative electrostatic micelles would repel the dianionic form of  
494 the dye [69,70]. Therefore, the differences found through these outcomes, comparing systems  
495 containing ERI or ERIs, can have a bearing at some level, with possible modification in the  
496 composition of predominant protolytic forms of ERI/ERIs as a function of the solubility  
497 balance and changes in pka values (due to the interaction of the drug with polox407/NaCMC  
498 and polox407/HPMC system). When incorporated to the polymer mixture studied, oxyethylene  
499 groups and cellulose derivatives can change the deprotonation equilibrium of phenolic and  
500 carboxylic groups of the PS, avoiding repulsion effects. The presence of ERI and ERIs in these  
501 mucoadhesive and thermoresponsive systems may foster a predominance of the neutral form  
502 of this dye by increasing their pKa, mainly in NaCMC gel, which presents increased negative  
503 electrostatic density. Additionally, ERI that presents both an ionization equilibrium and a  
504 solubility equilibrium, may major exist in its monoanionic form, while ERIs is in the dianionic  
505 one. Hence, the consideration of deprotonation equilibria may not follow the typical behaviour  
506 assumed by the Henderson-Hasselbalch equation which assumes that the chemical species is  
507 dilute in an aqueous environment [71].

508



#### 509 **4. Conclusion**

510 Polymeric blends composed of polox407 and HPMC or NaCMC were developed and  
511 their molecular structuration characterised for systems containing ERI or ERIs. Interaction  
512 studies demonstrated when the systems undergo micellisation drug molecules are converted  
513 into their monomeric form. By *in silico* study, ERIs has shown higher interaction with PEO  
514 than PPO. Moreover, systems composed of NaCMC and ERIs presented a repulsion effect due  
515 to its increased charge density, with polox407 structuration less impacted by the presence of  
516 HPMC. Morphological analysis evidenced the micelles had well-defined spherical structures,  
517 consistent with the native polox407. Calorimetry showed a reduction of polox407 crystallinity,  
518 CMT and enthalpy of micellisation when mixed with the cellulose derivatives, ERI or ERIs.  
519 Micellar size was evaluated by TEM, with NaCMC system reducing its micellar size, mainly  
520 in presence of ERI, while for HPMC significant changes were not observed. This retention of  
521 structure is crucial where encapsulation in micellar nanoparticles is commensurate to drug  
522 solubilisation, targeting, and cellular internalisation. Aiming toward photodynamic  
523 applications, these findings represent a rationale for understanding how the two states of the  
524 PS affect the polymeric blends and their micelle formation.

525

#### 526 **Acknowledgments**

527 The authors would like to thank the financial supports of CAPES (*Coordenação de*  
528 *Aperfeiçoamento de Pessoal de Nível Superior/Coordination for the Improvement of Higher*  
529 *Education of Brazil; n° 88881.361580/2019-01-PDSE program), CNPq (Conselho Nacional de*  
530 *Desenvolvimento Científico e Tecnológico/National Counsel of Technological and Scientific*  
531 *Development of Brazil; n° 307695/2020-4) and FINEP (Financiadora de Estudos e*  
532 *Projetos/Financier of Studies and Projects of Brazil). Also, the authors thank ORCA program*

533 system version 4.0, principally Dr. Holger Kruse and Dr. Andreas Hansen for their help and  
534 knowledge with the implementation of HF-3C into the ORCA program suit.

535

## 536 **References**

537 [1] S. Wood, D. Metcalf, D. Devine, C. Robinson, Erythrosine is a potential photosensitizer  
538 for the photodynamic therapy of oral plaque biofilms, *J. Antimicrob. Chemother.* 57  
539 (2006) 680–684. doi:10.1093/jac/dkl021.

540 [2] A.D. Garg, M. Bose, M.I. Ahmed, W.A. Bonass, S.R. Wood, In vitro studies on  
541 erythrosine-based photodynamic therapy of malignant and pre-malignant oral epithelial  
542 cells, *PLoS One.* 7 (2012) 1–12. doi:10.1371/journal.pone.0034475.

543 [3] D.S. Pellosi, B.M. Estevão, C.F. Freitas, T.M. Tsubone, W. Caetano, N. Hioka,  
544 Photophysical properties of erythrosin ester derivatives in ionic and non-ionic micelles,  
545 *Dye. Pigment.* 99 (2013) 705–712. doi:10.1016/j.dyepig.2013.06.026.

546 [4] L.M. Tokubo, P.L. Rosalen, J. de Cássia Orlandi Sardi, I.A. Freires, M. Fujimaki, J.E.  
547 Umeda, P.M. Barbosa, G.O. Tecchio, N. Hioka, C.F. de Freitas, R.S. Suga Terada,  
548 Antimicrobial effect of photodynamic therapy using erythrosine/methylene blue  
549 combination on *Streptococcus mutans* biofilm, *Photodiagnosis Photodyn. Ther.* 23  
550 (2018) 94–98. doi:10.1016/j.pdpdt.2018.05.004.

551 [5] C.A. Robertson, D.H. Evans, H. Abrahamse, Photodynamic therapy (PDT): A short  
552 review on cellular mechanisms and cancer research applications for PDT, *J. Photochem.*  
553 *Photobiol. B Biol.* 96 (2009) 1–8. doi:10.1016/j.jphotobiol.2009.04.001.

554 [6] National Library of Medicine HSDB Database, Erythrosine sodium, 27873 (2020).  
555 <https://toxnet.nlm.nih.gov/cgi-bin/sis/search/a?dbs+hsdb:@term+@DOCNO+7974>.

556 [7] D.S. Pellosi, B.M. Estevão, J. Semensato, D. Severino, M.S. Baptista, M.J. Politi, N.  
557 Hioka, W. Caetano, Photophysical properties and interactions of xanthene dyes in

- 558 aqueous micelles, *J. Photochem. Photobiol. A Chem.* 247 (2012) 8–15.  
559 doi:10.1016/j.jphotochem.2012.07.009.
- 560 [8] K. Plaetzer, T. Kiesslich, T. Verwanger, B. Krammer, The modes of cell death induced  
561 by PDT: An overview, *Med. Laser Appl.* 18 (2003) 7–19. doi:10.1078/1615-1615-  
562 00082.
- 563 [9] A.M. Bodratti, P. Alexandridis, Amphiphilic block copolymers in drug delivery:  
564 advances in formulation structure and performance, *Expert Opin. Drug Deliv.* 15 (2018)  
565 1085–1104. doi:10.1080/17425247.2018.1529756.
- 566 [10] P. Alexandridis, T. Alan Hatton, Poly(ethylene oxide)poly(propylene  
567 oxide)poly(ethylene oxide) block copolymer surfactants in aqueous solutions and at  
568 interfaces: thermodynamics, structure, dynamics, and modeling, *Colloids Surfaces A*  
569 *Physicochem. Eng. Asp.* 96 (1995) 1–46. doi:10.1016/0927-7757(94)03028-X.
- 570 [11] M.A. Abou-Shamat, J. Calvo-Castro, J.L. Stair, M.T. Cook, Modifying the Properties  
571 of Thermogelling Poloxamer 407 Solutions through Covalent Modification and the Use  
572 of Polymer Additives, *Macromol. Chem. Phys.* 220 (2019) 1–19.  
573 doi:10.1002/macp.201900173.
- 574 [12] G. Dumortier, N. El Kateb, M. Sahli, S. Kedjar, A. Boulliat, J.C. Chaumeil,  
575 Development of a thermogelling ophthalmic formulation of cysteine, *Drug Dev. Ind.*  
576 *Pharm.* 32 (2006) 63–72. doi:10.1080/03639040500390934.
- 577 [13] M. Dewan, G. Sarkar, M. Bhowmik, B. Das, A.K. Chattoopadhyay, D. Rana, D.  
578 Chattopadhyay, Effect of gellan gum on the thermogelation property and drug release  
579 profile of Poloxamer 407 based ophthalmic formulation, *Int. J. Biol. Macromol.* 102  
580 (2017) 258–265. doi:10.1016/j.ijbiomac.2017.03.194.
- 581 [14] K. da S.S. Campanholi, A.P. Gerola, B.H. Vilsinski, É.L. de Oliveira, F.A.P. de Moraes,  
582 B.R. Rabello, G. Braga, I.R. Calori, E.L. Silva, N. Hioka, W. Caetano, Development of

- 583 Pluronic® nanocarriers comprising Pheophorbide, Zn-Pheophorbide, Lapachol and  $\beta$ -  
584 lapachone combined drugs: Photophysical and spectroscopic studies, *Dye. Pigment.* 157  
585 (2018) 238–250. doi:10.1016/j.dyepig.2018.04.057.
- 586 [15] D. Szweda, R. Szweda, A. Dworak, B. Trzebicka, Thermoresponsive  
587 poly[oligo(ethylene glycol) methacrylate]s and their bioconjugates - Synthesis and  
588 solution behavior, *Polimery/Polymers.* 62 (2017) 298–310.  
589 doi:10.14314/polimery.2017.298.
- 590 [16] M.L. Bruschi, D.S. Jones, H. Panzeri, M.P.D. Gremião, O. de Freitas, E.H.G. Lara,  
591 Semisolid Systems Containing Propolis for the Treatment of Periodontal Disease: In  
592 Vitro Release Kinetics, Syringeability, Rheological, Textural and Mucoadhesive  
593 Properties, *J. Pharm. Sci.* 99 (2007) 4215–4227. doi:10.1002/jps.
- 594 [17] D.S. Jones, M.L. Bruschi, O. de Freitas, M.P.D. Gremião, E.H.G. Lara, G.P. Andrews,  
595 Rheological, mechanical and mucoadhesive properties of thermoresponsive,  
596 bioadhesive binary mixtures composed of poloxamer 407 and carbopol 974P designed  
597 as platforms for implantable drug delivery systems for use in the oral cavity, *Int. J.*  
598 *Pharm.* 372 (2009) 49–58. doi:10.1016/j.ijpharm.2009.01.006.
- 599 [18] M. V. Junqueira, F.B. Borghi-Pangoni, S.B.S. Ferreira, B.R. Rabello, N. Hioka, M.L.  
600 Bruschi, Functional Polymeric Systems as Delivery Vehicles for Methylene Blue in  
601 Photodynamic Therapy, *Langmuir.* 32 (2016) 19–27.  
602 doi:10.1021/acs.langmuir.5b02039.
- 603 [19] K. da Silva Souza Campanholi, J.M. Jaski, R.C. da Silva Junior, A.B. Zanqui, D.  
604 Lazarin-Bidóia, C.M. da Silva, E.A. da Silva, N. Hioka, C.V. Nakamura, L. Cardozo-  
605 Filho, W. Caetano, Photodamage on *Staphylococcus aureus* by natural extract from  
606 *Tetragonia tetragonoides* (Pall.) Kuntze: Clean method of extraction, characterization  
607 and photophysical studies, *J. Photochem. Photobiol. B Biol.* (2020).

- 608 doi:10.1016/j.jphotobiol.2019.111763.
- 609 [20] F.B. Borghi-Pangoni, M.V. Junqueira, S.B. de Souza Ferreira, L.L. Silva, B.R. Rabello,  
610 L.V. de Castro, M.L. Baesso, A. Diniz, W. Caetano, M.L. Bruschi, Preparation and  
611 characterization of bioadhesive system containing hypericin for local photodynamic  
612 therapy, *Photodiagnosis Photodyn. Ther.* 19 (2017) 284–297.  
613 doi:10.1016/j.pdpdt.2017.06.016.
- 614 [21] W. Wang, P.C.L. Hui, E. Wat, F.S.F. Ng, C.W. Kan, X. Wang, E.C.W. Wong, H. Hu,  
615 B. Chan, C.B.S. Lau, P.C. Leung, In vitro drug release and percutaneous behavior of  
616 poloxamer-based hydrogel formulation containing traditional Chinese medicine,  
617 *Colloids Surfaces B Biointerfaces.* 148 (2016) 526–532.  
618 doi:10.1016/j.colsurfb.2016.09.036.
- 619 [22] C. Pagano, S. Giovagnoli, L. Perioli, M.C. Tiralti, M. Ricci, Development and  
620 characterization of mucoadhesive-thermoresponsive gels for the treatment of oral  
621 mucosa diseases, *Eur. J. Pharm. Sci.* 142 (2020) 105125.  
622 doi:10.1016/j.ejps.2019.105125.
- 623 [23] J.B. da Silva, M.T. Cook, M.L. Bruschi, Thermo-responsive systems composed of  
624 poloxamer 407 and HPMC or NaCMC: mechanical, rheological and sol-gel transition  
625 analysis, *Carbohydr. Polym.* 240 (2020) 116268. doi:10.1016/j.carbpol.2020.116268.
- 626 [24] J.B. da Silva, R.S. dos Santos, M.B. da Silva, G. Braga, M.T. Cook, M.L. Bruschi,  
627 Interaction between mucoadhesive cellulose derivatives and Pluronic F127:  
628 Investigation on the micelle structure and mucoadhesive performance, *Mater. Sci. Eng.*  
629 *C.* 119 (2021). doi:10.1016/j.msec.2020.111643.
- 630 [25] D.S. Jones, A.D. Woolfson, J. Djokic, Texture profile analysis of bioadhesive polymeric  
631 semisolids: Mechanical characterization and investigation of interactions between  
632 formulation components, *J. Appl. Polym. Sci.* 61 (1996) 2229–2234.

- 633 doi:10.1002/(SICI)1097-4628(19960919)61:12.
- 634 [26] H. Hägerström, K. Edsman, Interpretation of mucoadhesive properties of polymer,  
635 (2001) 1589–1599. doi:10.1211/0022357011778197.
- 636 [27] V.R. Batistela, D.S. Pellosi, F.D. De Souza, W.F. Da Costa, S.M. De Oliveira Santin,  
637 V.R. De Souza, W. Caetano, H.P.M. De Oliveira, I.S. Scarminio, N. Hioka, PKa  
638 determinations of xanthene derivates in aqueous solutions by multivariate analysis  
639 applied to UV-Vis spectrophotometric data, *Spectrochim. Acta - Part A Mol. Biomol.*  
640 *Spectrosc.* 79 (2011) 889–897. doi:10.1016/j.saa.2011.03.027.
- 641 [28] National Library of Medicine HSDB Database, Erythrosine B, (2013) 2–4.
- 642 [29] I.R. Schmolka, Artificial skin I. Preparation and properties of Pluronic F127 Gels for  
643 treatment of burns, *J. Biomed. Mater. Res.* 6 (1972) 571–582.  
644 doi:10.1002/jbm.820060609.
- 645 [30] S.B. De Souza Ferreira, J. Bassi da Silva, F.B. Borghi-Pangoni, M.V. Junqueira, M.L.  
646 Bruschi, Linear correlation between rheological, mucoadhesive and textural properties  
647 of thermoresponsive polymer blends for biomedical applications, *J. Mech. Behav.*  
648 *Biomed. Mater.* 55 (2015) 164–178. doi:10.1016/j.jmbbm.2015.10.026.
- 649 [31] J. Bassi da Silva, V. V Khutoryanskiy, M.L. Bruschi, M.T. Cook, A mucosa-mimetic  
650 material for the mucoadhesion testing of thermogelling semi-solids, *Int. J. Pharm.* 528  
651 (2017) 586–594. doi:10.1016/j.ijpharm.2017.06.025.
- 652 [32] D.S. Pellosi, B.M. Estevão, J. Semensato, D. Severino, M.S. Baptista, M.J. Politi, N.  
653 Hioka, W. Caetano, Photophysical properties and interactions of xanthene dyes in  
654 aqueous micelles, *J. Photochem. Photobiol. A Chem.* 247 (2012) 8–15.  
655 doi:10.1016/j.jphotochem.2012.07.009.
- 656 [33] P.C. de S. Pereira, P.F. do A. Costa, D.S. Pellosi, I.R. Calori, B.H. Vilsinski, B.M.  
657 Estevão, N. Hioka, W. Caetano, Photophysical properties and interaction studies of Rose

658 Bengal derivatives with biomimetic systems based in micellar aqueous solutions, *J. Mol.*  
659 *Liq.* 230 (2017) 674–685. doi:10.1016/j.molliq.2017.01.055.

660 [34] F. Neese, Software update : the ORCA program system , version 4 . 0, (2017) 1–6.  
661 doi:10.1002/wcms.1327.

662 [35] R. Sure, S. Grimme, Corrected small basis set Hartree-Fock method for large systems,  
663 *J. Comput. Chem.* 34 (2013) 1672–1685. doi:10.1002/jcc.23317.

664 [36] M.D. Hanwell, D.E. Curtis, D.C. Lonie, T. Vandermeersch, E. Zurek, G.R. Hutchison,  
665 Avogadro : An advanced semantic chemical editor , visualization , and analysis  
666 platform, *J. Cheminform.* (2012) 33. doi:10.1186/1758-2946-4-17.

667 [37] R.S. Gonçalves, G. Braga, A.C. V. de Oliveira, G.B. César, T.T. Tominaga, E.H.  
668 Zampiere, I.R. Calori, F.A.P. de Morais, E.A. Basso, R.M. Pontes, N. Hioka, W.  
669 Caetano, Hypericin Delivery System Based on P84 Copolymeric Micelles Linked with  
670 N -(3-Aminopropyl)-2-pyrrolidone for Melanoma-Targeted Photodynamic Therapy,  
671 *ACS Appl. Polym. Mater.* 2 (2020) 1692–1701. doi:10.1021/acsapm.0c00114.

672 [38] V. Enev, P. Sedláček, S. Jarábková, T. Velcer, M. Pekař, ATR-FTIR spectroscopy and  
673 thermogravimetry characterization of water in polyelectrolyte-surfactant hydrogels,  
674 *Colloids Surfaces A Physicochem. Eng. Asp.* 575 (2019) 1–9.  
675 doi:10.1016/j.colsurfa.2019.04.089.

676 [39] S.J. Lue, D.T. Lee, J.Y. Chen, C.H. Chiu, C.C. Hu, Y.C. Jean, J.Y. Lai, Diffusivity  
677 enhancement of water vapor in poly(vinyl alcohol)-fumed silica nano-composite  
678 membranes: Correlation with polymer crystallinity and free-volume properties, *J.*  
679 *Memb. Sci.* 325 (2008) 831–839. doi:10.1016/j.memsci.2008.09.015.

680 [40] H. Liu, P. Yang, D. Wan, The accessibility of a unimolecular micelle’s core to  
681 environmental ions: Exploration with a xanthene dye, *J. Polym. Sci. Part B Polym. Phys.*  
682 53 (2015) 566–573. doi:10.1002/polb.23671.

- 683 [41] F.A.P. de Morais, R.S. Gonçalves, B.H. Vilsinski, É.L. de Oliveira, N.L. Rocha, N.  
684 Hioka, W. Caetano, Hypericin photodynamic activity in DPPC liposome. PART I:  
685 biomimetism of loading, location, interactions and thermodynamic properties, J.  
686 Photochem. Photobiol. B Biol. 190 (2019) 118–127.  
687 doi:10.1016/j.jphotobiol.2018.11.019.
- 688 [42] D. Pentak, Z. Zawada, A. Szkudlarek, A. Ploch, M. Maciążek-Jurczyk, Determination  
689 of the fluorescence labels location in lipid bilayer based on fluorescence quenching, J.  
690 Mol. Liq. 256 (2018) 84–89. doi:10.1016/j.molliq.2018.02.027.
- 691 [43] G. Ramírez-Galicia, R. Garduño-Juárez, M. Gabriela Vargas, Effect of water molecules  
692 on the fluorescence enhancement of Aflatoxin B1 mediated by Aflatoxin B1:beta-  
693 cyclodextrin complexes. A theoretical study., Photochem. Photobiol. Sci. 6 (2007) 110–  
694 118. doi:10.1039/b614107b.
- 695 [44] M.S. Bakshi, S. Sachar, Influence of temperature on the mixed micelles of Pluronic F127  
696 and P103 with dimethylene-bis-(dodecyldimethylammonium bromide), J. Colloid  
697 Interface Sci. 296 (2006) 309–315. doi:10.1016/j.jcis.2005.09.008.
- 698 [45] T. Bayraktutan, Investigation of photophysical and binding properties of Rose Bengal  
699 dye on graphene oxide and polyethyleneimine-functionalized graphene oxide  
700 nanocomposites, Chem. Pap. 74 (2020) 3017–3024. doi:10.1007/s11696-020-01130-4.
- 701 [46] B.B. Bhowmik, P. Ganguly, Photophysics of xanthene dyes in surfactant solution,  
702 Spectrochim. Acta Part A Mol. Biomol. Spectrosc. 61 (2005) 1997–2003.  
703 doi:10.1016/j.saa.2004.07.031.
- 704 [47] G. Baek, C. Kim, Rheological properties of Carbopol containing nanoparticles, J. Rheol.  
705 (N. Y. N. Y). 55 (2011) 313–330. doi:10.1122/1.3538092.
- 706 [48] P. Shrimal, G. Jadeja, J. Naik, S. Patel, Continuous microchannel precipitation to  
707 enhance the solubility of telmisartan with poloxamer 407 using Box-Behnken design



- 708 approach, *J. Drug Deliv. Sci. Technol.* 53 (2019) 101225.  
709 doi:10.1016/j.jddst.2019.101225.
- 710 [49] I. Ahemen, Effect of Sodium Carboxymethyl Cellulose Concentration on the  
711 Photophysical Properties of Zinc Sulfide Nanoparticles, *Br. J. Appl. Sci. Technol.* 3  
712 (2013) 1228–1245. doi:10.9734/bjast/2014/3803.
- 713 [50] M.N. Chai, M.I.N. Isa, The Oleic Acid Composition Effect on the Carboxymethyl  
714 Cellulose Based Biopolymer Electrolyte, *J. Cryst. Process Technol.* 03 (2013) 1–4.  
715 doi:10.4236/jcpt.2013.31001.
- 716 [51] P. Tonglairoum, T. Rojanarata, T. Ngawhirunpat, P. Akkaramongkolporn, R.  
717 Kaomongkolgit, P. Opanasopit, Erythrosine Incorporated Fast-Dissolving Patches for  
718 Dental Plaque Disclosing, *Adv. Pharmacol. Pharm.* 5 (2017) 12–19.  
719 doi:10.13189/app.2017.050102.
- 720 [52] M. El-Badry, M.A. Hassan, M.A. Ibrahim, H. Elsaghir, Performance of poloxamer 407  
721 as hydrophilic carrier on the binary mixtures with nimesulide, *Farmacia.* 61 (2013)  
722 1137–1150.
- 723 [53] L. Djekic, B. Čalića, Đ. Medarević, Gelation behavior, drug solubilization capacity and  
724 release kinetics of poloxamer 407 aqueous solutions: The combined effect of copolymer,  
725 cosolvent and hydrophobic drug, *J. Mol. Liq.* 303 (2020).  
726 doi:10.1016/j.molliq.2020.112639.
- 727 [54] H. Tsuji, I. Fukui, Enhanced thermal stability of poly(lactide)s in the melt by  
728 enantiomeric polymer blending, *Polymer (Guildf).* 44 (2003) 2891–2896.  
729 doi:10.1016/S0032-3861(03)00175-7.
- 730 [55] P. Gill, T.T. Moghadam, B. Ranjbar, Differential scanning calorimetry techniques:  
731 Applications in biology and nanoscience, *J. Biomol. Tech.* 21 (2010) 167–193.
- 732 [56] A.M. Pragatheeswaran, S.B. Chen, Effect of chain length of PEO on the gelation and

- 733 micellization of the pluronic F127 copolymer aqueous system, *Langmuir*. 29 (2013)  
734 9694–9701. doi:10.1021/la401639g.
- 735 [57] K. Al Khateb, E.K. Ozhmukhametova, M.N. Mussin, S.K. Seilkhanov, T.K.  
736 Rakhypbekov, W.M. Lau, V. V. Khutoryanskiy, In situ gelling systems based on  
737 Pluronic F127/Pluronic F68 formulations for ocular drug delivery, *Int. J. Pharm.* 502  
738 (2016) 70–79. doi:10.1016/j.ijpharm.2016.02.027.
- 739 [58] P. Alexandridis, J.F. Holzwarth, T.A. Hatton, Micellization of Poly(ethylene oxide)-  
740 Poly(propylene oxide)-Poly(ethylene oxide) Triblock Copolymers in Aqueous  
741 Solutions: Thermodynamics of Copolymer Association, *Macromolecules*. 27 (1994)  
742 2414–2425. doi:10.1021/ma00087a009.
- 743 [59] J. Jiang, C. Li, J. Lombardi, R.H. Colby, B. Rigas, M.H. Rafailovich, J.C. Sokolov, The  
744 effect of physiologically relevant additives on the rheological properties of concentrated  
745 Pluronic copolymer gels, *Polymer (Guildf)*. 49 (2008) 3561–3567.  
746 doi:10.1016/j.polymer.2008.05.038.
- 747 [60] L.C. Pham Trong, M. Djabourov, A. Ponton, Mechanisms of micellization and rheology  
748 of PEO-PPO-PEO triblock copolymers with various architectures, *J. Colloid Interface*  
749 *Sci.* 328 (2008) 278–287. doi:10.1016/j.jcis.2008.09.029.
- 750 [61] M. Zhang, M. Djabourov, C. Bourgaux, K. Bouchemal, Nanostructured fluids from  
751 pluronic® mixtures, *Int. J. Pharm.* 454 (2013) 599–610.  
752 doi:10.1016/j.ijpharm.2013.01.043.
- 753 [62] A.M. Pragatheeswaran, S.B. Chen, The influence of poly(acrylic acid) on micellization  
754 and gelation characteristics of aqueous Pluronic F127 copolymer system, *Colloid*  
755 *Polym. Sci.* 294 (2016) 107–117. doi:10.1007/s00396-015-3757-7.
- 756 [63] S.K. Nixon, S. Hvidt, C. Booth, Micellization of block copolymer P94 in aqueous  
757 solution, *J. Colloid Interface Sci.* 280 (2004) 219–223. doi:10.1016/j.jcis.2004.07.031.

- 758 [64] N.M.P.S. Ricardo, N.M.P.S. Ricardo, F. de M.L.L. Costa, F.W.A. Bezerra, C.  
759 Chaibundit, D. Hermida-Merino, B.W. Greenland, S. Burattini, I.W. Hamley, S. Keith  
760 Nixon, S.G. Yeates, Effect of water-soluble polymers, polyethylene glycol and  
761 poly(vinylpyrrolidone), on the gelation of aqueous micellar solutions of Pluronic  
762 copolymer F127, *J. Colloid Interface Sci.* 368 (2012) 336–341.  
763 doi:10.1016/j.jcis.2011.10.062.
- 764 [65] C.F. de Freitas, D. Vanzin, T.L. Braga, D.S. Pellosi, V.R. Batistela, W. Caetano, N.  
765 Hioka, Multivariate analysis of protolytic and tautomeric equilibria of Erythrosine B and  
766 its ester derivatives in ionic and non-ionic micelles, *J. Mol. Liq.* 313 (2020) 113320.  
767 doi:10.1016/j.molliq.2020.113320.
- 768 [66] R.S.C.M.Q. Antonino, T.L. Nascimento, E.R. de Oliveira Junior, L.G. Souza, A.C.  
769 Batista, E.M. Lima, Thermoreversible mucoadhesive polymer-drug dispersion for  
770 sustained local delivery of budesonide to treat inflammatory disorders of the GI tract, *J.*  
771 *Control. Release.* 303 (2019) 12–23. doi:10.1016/j.jconrel.2019.04.011.
- 772 [67] P.K. Sharma, S.R. Bhatia, Effect of anti-inflammatories on Pluronic® F127: Micellar  
773 assembly, gelation and partitioning, *Int. J. Pharm.* 278 (2004) 361–377.  
774 doi:10.1016/j.ijpharm.2004.03.029.
- 775 [68] P.R. Desai, N.J. Jain, R.K. Sharma, P. Bahadur, Effect of additives on the micellization  
776 of PEO/PPO/PEO block copolymer F127 in aqueous solution, *Colloids Surfaces A*  
777 *Physicochem. Eng. Asp.* 178 (2001) 57–69. doi:10.1016/S0927-7757(00)00493-3.
- 778 [69] C.F. de Freitas, D.S. Pellosi, B.M. Estevão, I.R. Calori, T.M. Tsubone, M.J. Politi, W.  
779 Caetano, N. Hioka, Nanostructured Polymeric Micelles Carrying Xanthene Dyes for  
780 Photodynamic Evaluation, *Photochem. Photobiol.* 92 (2016) 790–799.  
781 doi:10.1111/php.12645.
- 782 [70] M.A.S. Fernández, P. Fromherz, Lipoid pH indicators as probes of electrical potential

783 and polarity in micelles, *J. Phys. Chem.* 81 (1977) 1755–1761.  
784 doi:10.1021/j100533a009.

785 [71] J. Reijenga, A. van Hoof, A. van Loon, B. Teunissen, Development of methods for the  
786 determination of pKa values, *Anal. Chem. Insights.* 8 (2013) 53–71.  
787 doi:10.4137/ACIS12304.

788